Nonlinear Dynamics and Systems Theory, **20** (2) (2020) 153–167

Sensorless Two Series Connected Quasi Six-Phase IM Based Direct Torque Control for Torque Ripples Minimization

Y. Chedni [1], DJ. Boudana [1], A. Moualdia [2*], L. Nezli [1] and P. Wira [3]

[1] *Process Control Laboratory, National Polytechnic School. Algiers, Algeria*
[2] *Laboratory of Electrical Engineering and Automatics (LREA), University of Medea, Algeria*
[3] *IRIMAS, Laboratory of Modeling Intelligence Process Systems (MIPS), University of Haute Alsace, Mulhouse, France.*

Received: November 17, 2019; Revised: March 7, 2020

Abstract: In this paper, a new direct torque control (DTC) is proposed for a two series connected quasi six-phase induction motor (IM) with sinusoidal distributed windings fed by a single six-phase voltage source inverter (VSI). The developed DTC control is reformulated as a variable structure control strategy characterized by its simplicity, fast response and robustness to motor parameter variations. Indeed, the proposed DTC controller accomplishes two tasks, first it guarantees a decoupled torque/flux control for each machine while imposing separate control loops, the second is to eliminate current circulation that appears in stator windings of each machine through the usage of appropriate vector maps in $(\alpha - \beta)$ and $(x - y)$ plan. The effectiveness and the robustness of the proposed method are shown by computer simulation.

Keywords: *direct torque control; voltage source inverter; two series connected quasi six-phase induction motor drive.*

Mathematics Subject Classification (2010): 03B52, 93C42, 94D05.

* Corresponding author: mailto:amoualdia@gmail.com

1 Introduction

Technological developments have allowed us to put in place the concept of multiplying the number of phases over three. This is to allow to reach important technical points. Firstly, the distribution of the total power over a large number of arms will allow a better dimensioning of the inverters enabling them to operate with high frequency [1–3]. Secondly, this multiplication of phases allows machines to continue working, even if one or more arms fail operating, till the fault is fixed. Thirdly, the analysis of the stator F.M.M has made it possible to highlight a crucial item, the more the phase multiplication increases, the more interaction between time and space harmonics will be pushed back to its higher ranks [3, 4]. Another important and practical point is the possibility of controlling two or more machines separately fed by a unique single voltage source inverter (VSI), when connected in series with an appropriate phase transposition, something which would always be beyond the reach in the case of three-phase machines; mainly where only parallel structure is allowed under certain strict conditions such as the usage of identical machines possessing equal power ratings when being fed by a single inverter as mentioned in [2]. Moreover, multi-phase systems enhance the series connected topology even when machines in the group are different as it had been demonstrated in the work [5]. The dual star induction motor (DSIM) is an example of this type of machines (two sets of stator windings with 30 deg displacement), it has the property of being easily rebuilt from a simple three-phase machine, but characterized by the fact that it is better than the three-phase machine, when the torque ripples and the rotor losses have to be considered. Despite its reputation, the dual star machine, unfortunately, undergoes a problem characterized by the appearance of stator circulation currents when it is fed through a voltage source inverter as described in [6, 7]. Another challenge is added to the precedent drawback in the case of two series connected dual star machine, therefore, a compromise will be imposed between advantages and the multiplication of the losses generated by the series structure by non-producing torque/flux components if compared with a single machine. Underlying the literature review, a chain of important empirical works have been realized dealing with different types of multi-phase multi-machines such as series connected five-phase, symmetrical six-three phase. In [5], the shortcoming had been resolved in such a way, when one machine in the group operates at low speed with high torque (high current) and the other machine will operate at high speed (high voltage) with low torque, consequently, the total stator copper losses remain less than or equal to the rated value of one machine, however, this solution is still not generalized in the case where the number of machines increases. Direct torque control, or DTC as it is called, is the very latest AC drive technology developed by manufactures in the world consequently after Blaschke and his colleague Depenbrock's research came into sight in 1971. DTC allows the motor torque and stator flux to be used as primary control variables, both of which are obtained directly from the motor itself [8]. The advantages of DTC technology over the traditional AC drive can be summarized as follows. First, a fast torque response can be achieved which will significantly reduce the speed drop time during a load transient, bringing much improved process control and a more consistent product quality, then, it permits torque's control at low frequencies, which is particularly beneficial to cranes or elevators, where the load needs to be started and stopped regularly without any jerking. Moreover, torque linearity, this property is very important in precision application such as winders, where an accurate and consistent level of winding is critical. Another important advantage to be mentioned, is the dynamic speed accuracy

during a sudden load change, helping the drive to quickly recover its stable state. When compared to the other vector control drives, the direct torque control brings the cost saving benefit since no tachometer or feedback is needed. Despite all these advantages, the DTC is still facing considerable drawbacks such as variable switching frequencies and torque ripple because of the use of hysteresis controllers for torque and flux [8–10]. For such reasons, lots of research are being undertaken constantly aiming to develop technical remedy for these disadvantages. In the three phase systems, there exist only eight possible inverter states, while a large number of inverter states depending on the number of phases in the multiphase systems can be found such as 64 states for six phases, 32 states for five phases. This additional degree of freedom allows considerable flexibility in their selection, therefore, finer adjustment of flux and torque could be achieved [11]. Nevertheless, this property requires a special attention and a complex criterion when synthesizing switching lookup tables. Various research have been presented on switching lookup table based direct torque control. In [12], the concept of virtual voltage was introduced to achieve cancellation of low order harmonic currents for a single five-phase induction motor. Another research was presented in [6], where three lookup tables have been implemented for a single split phase induction motor (SPIM) to suppress zero sequence current components. The principle of control decoupling of a two series connected dual star motor drive lies in the fact that the $(\alpha - \beta)$ components of the six-phase VSI control the first motor and the $(x - y)$ components will control the second one. Hence, for the first motor, the $(\alpha - \beta)$ inverter components appear as responsible of producing flux/torque while the $(x - y)$ components appear as non-flux/torque producing and only generate losses. On the contrary, the $(x - y)$ components appear as responsible of producing flux/torque for the second machine while the $(\alpha - \beta)$ only generate losses [3, 5]. In this paper, an extension was made on two series connected dual star induction motor fed by a single six-phase voltage source inverter (VSI) while preserving the technique developed in [6]. Therefore, the proposed DTC controller adopted here aims, on one hand, at ensuring a decoupled flux/torque control for each machine within the group while imposing independent control of the two series connected drive system. On the other hand, it should eliminate the components flowing in each machine, that do not contribute in producing flux/torque but only increase copper losses through a proper selection of virtual voltage vectors. Additionally, to overcome the problems caused by flux/ torque estimators which usually deteriorate the system performances such as those related to signal integration and dc-drift caused by the initial integral condition [12, 13], an adaptive variable observer based on the Lypunov theory was introduced to improve the proposed controller performances. A number of computer simulations are achieved as a comparative study with the conventional DTC controller, where only large vector maps in $(\alpha - \beta)$ and $(x - y)$ plan are used to demonstrate the impact of the proposed controller on torque ripples minimization and current harmonics cancellation.

2 Modelling of the Drive System

This section is devoted to the modelling of two series connected dual-star induction motor (DSIM1) and (DSIM2), respectively, for first and second machine or simply quasi six-phases squirrel cage induction motors where stator winding of each machine is displaced in space by 30 degrees. The two motor drives are connected in series through an appropriate phase transposition and fed by a single six-phase voltage source inverter (VSI) as shown in Fig. 1. The neutral points n1, n2 of the two windings are normally kept isolated to

prevent the stator current harmonics of the order divisible by three from flowing [5]. The

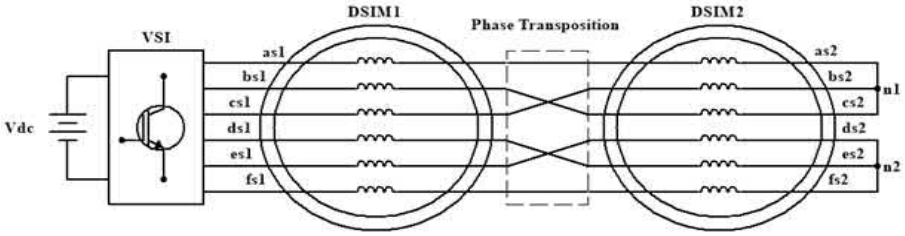

Figure 1: Drive system block diagram.

relation between voltages and currents can be given as

$$\begin{aligned} V_A &= v_{as1} + v_{as2}, \quad i_A = i_{as1} = i_{as2}, \\ V_B &= v_{bs1} + v_{cs2}, \quad i_B = i_{bs1} = i_{cs2}, \\ V_C &= v_{cs1} + v_{bs2}, \quad i_C = i_{cs1} = i_{bs2}, \\ V_D &= v_{ds1} + v_{es2}, \quad i_D = i_{ds1} = i_{es2}, \\ V_E &= v_{es1} + v_{ds2}, \quad i_E = i_{es1} = i_{ds2}, \\ V_F &= v_{fs1} + v_{fs2}, \quad i_F = i_{fs1} = i_{fs2}, \end{aligned} \tag{1}$$

by using the decoupling power-invariant transformation matrix

$$C = \frac{1}{\sqrt{3}} \cdot \begin{bmatrix} 1 & \cos(4\alpha) & \cos(8\alpha) & \cos(\alpha) & \cos(5\alpha) & \cos(9\alpha) \\ 0 & \sin(4\alpha) & \sin(8\alpha) & \sin(\alpha) & \sin(5\alpha) & \sin(9\alpha) \\ 1 & \cos(8\alpha) & \cos(4\alpha) & \cos(5\alpha) & \cos(\alpha) & cos(9\alpha) \\ 0 & \sin(8\alpha) & \sin(4\alpha) & \sin(5\alpha) & \sin(\alpha) & \sin(9\alpha) \\ 1 & 1 & 1 & 0 & 0 & 0 \\ 0 & 0 & 0 & 1 & 1 & 1 \end{bmatrix}, \tag{2}$$

where $\alpha = \frac{\pi}{6}$, the original phase variables are transformed to new $(\alpha - \beta)$ and $(x - y)$ variables as

$$\begin{bmatrix} v_{\alpha}^{inv} \\ v_{\beta}^{inv} \\ v_{x}^{inv} \\ v_{y}^{inv} \\ v_{o+}^{inv} \\ v_{o-}^{inv} \end{bmatrix} = C \begin{bmatrix} v_{as1} + v_{as2} \\ v_{bs1} + v_{cs2} \\ v_{cs1} + v_{bs2} \\ v_{ds1} + v_{es2} \\ v_{es1} + v_{ds2} \\ v_{fs1} + v_{fs2} \end{bmatrix} = \begin{bmatrix} v_{\alpha s1} + v_{xs2} \\ v_{\beta s1} + v_{ys2} \\ v_{xs1} + v_{\alpha s2} \\ v_{ys1} + v_{\beta s2} \\ 0 \\ 0 \end{bmatrix}, \tag{3}$$

$$\begin{aligned} i_{\alpha}^{inv} &= i_{\alpha s1} = i_{xs2}, \\ i_{\beta}^{inv} &= i_{\beta s1} = i_{ys2}, \\ i_{x}^{inv} &= i_{xs1} = i_{\alpha s2}, \\ i_{y}^{inv} &= i_{ys1} = i_{\beta s2}. \end{aligned} \tag{4}$$

Torque equations of two series connected machines are given as follows:

$$T_{ek} = P_k L_{mk} (i_{\alpha rk} i_{\beta sk} - i_{\beta rk} i_{\alpha sk}), \tag{5}$$

where $k = 1, 2$ and P_k is a pole pair. The stator voltage equations of each machine are

$$\begin{aligned} v_{\alpha sk} &= R_{sk} i_{\alpha sk} + \frac{d}{dt}(L_{sk} i_{\alpha sk} + L_{mk} i_{\alpha rk}), \\ v_{\beta sk} &= R_{sk} i_{\beta sk} + \frac{d}{dt}(L_{sk} i_{\alpha sk} + L_{mk} i_{\alpha rk}), \\ v_{xsk} &= R_{sk} i_{xsk} + \frac{d}{dt}(L_{lsk} i_{xsk}), \\ v_{ysk} &= R_{sk} i_{ysk} + \frac{d}{dt}(L_{lsk} i_{ysk}). \end{aligned} \tag{6}$$

The rotor voltage equations of each machine are

$$\begin{aligned} 0 &= R_{rk} i_{\alpha rk} + \omega_{rk}(L_{rk} i_{\beta rk} + + L_{mk} i_{\beta sk}) + \frac{d}{dt}(L_{rk} i_{\alpha rk} + L_{mk} i_{\alpha sk}), \\ 0 &= R_{rk} i_{\beta rk} - \omega_{rk}(L_{rk} i_{\alpha rk} + L_{mk} i_{\alpha sk}) + \frac{d}{dt}(L_{rk} i_{\beta rk} + L_{mk} i_{\beta sk}), \end{aligned} \tag{7}$$

where $k = 1, 2$. From (4) and (5) one can see that the currents producing flux/torque for the first machine $(i_{\alpha s1}, i_{\beta s1})$ appear as non producing flux/torque for the second one and vice versa. As a result, the two series connected machine can be controlled independently.

3 Design of Direct Torque Controller

3.1 Conventional DTC controller

For a two level six-phase inverter feeding the two-motor drive system under study there are 64 possible inverter states which are defined as $[s_a, s_b, s_c, s_d, s_e, s_f]$ for the upper switches, while the lower inverter states must operate in a complementary mode with the upper ones in each leg [5].

$$\underline{v}_{\alpha\beta}^{inv} = \frac{2}{6}(v_a + \underline{a}^4 v_b + \underline{a}^8 v_c + \underline{a} v_d + \underline{a}^5 v_e + \underline{a}^9 v_f), \tag{8}$$

$$\underline{v}_{xy}^{inv} = \frac{2}{6}(v_a + \underline{a}^8 v_b + \underline{a}^4 v_c + \underline{a}^5 v_d + \underline{a} v_e + \underline{a}^9 v_f), \tag{9}$$

where $\underline{a} = exp(j\frac{\pi}{6})$.

According to (8) and (9), the six-phase voltages of each inverter state are transformed into two voltage vectors $\underline{v}_{\alpha\beta}^{inv}$ and $\underline{v}_{xy}^{inv}$. Zero-sequence can not be excited because of the star connection, therefore it is omitted. These two voltage vectors are plotted in their associated $(\alpha - \beta)$ and $(x - y)$ sub-space as shown in Figure 2. Each plan comprises four dodecahedrons with magnitude of $\frac{\sqrt{2}(\sqrt{3}+1)}{6}.v_{dc}$, $\frac{\sqrt{2}(\sqrt{3}-1)}{6}.v_{dc}$, $\frac{\sqrt{2}}{3}.v_{dc}$, $\frac{1}{3}.v_{dc}$, and they are classified according to their magnitude into five types: null, smallest, small, largest and large. In total, there exist 64 vectors in each plan. Inverter states which are given in binary form have been coded in octal system for better representation, for example, states (100100) have been coded to (44) and mentioned as v_{44} in Figure 2.

Same technique has been applied for all vectors in each plan. The conventional DTC diagram is shown in Figure 3. Correct inverter states that should be used are based on the stator flux and torque errors. Three-level and two-level hysteresis regulators are used, respectively, for torque and flux. The position information of the stator flux linkage is

required to define sectors for each machine. Voltage lookup tables of conventional DTC for each motor in the group are built using only the largest vector maps in $(\alpha - \beta)$ and $(x - y)$ plan for fully using available DC bus ($\frac{\sqrt{2}(\sqrt{3}+1)}{6}.v_{dc}$) without any compensation. The aim of this sub-section is to show the impact of using only the largest vectors from sub-space $(\alpha - \beta)$ and $(x - y)$ for lookup tables to control, respectively, DSIM1 and DSIM2.

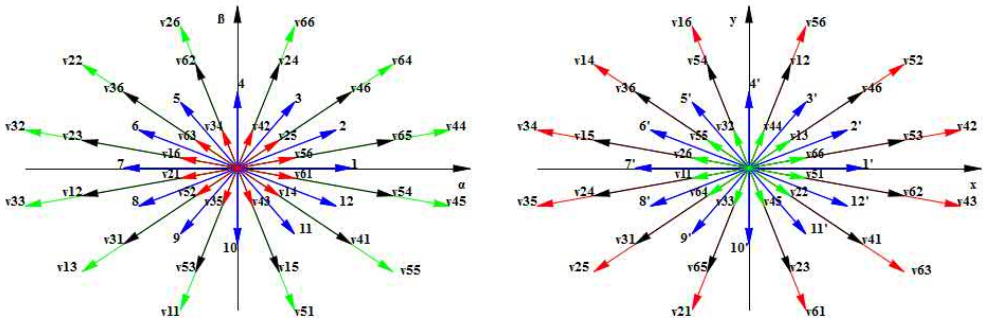

Figure 2: Distribution of basic space vectors: (a) for $(\alpha - \beta)$ plan and (b) for $(x - y)$ plan.

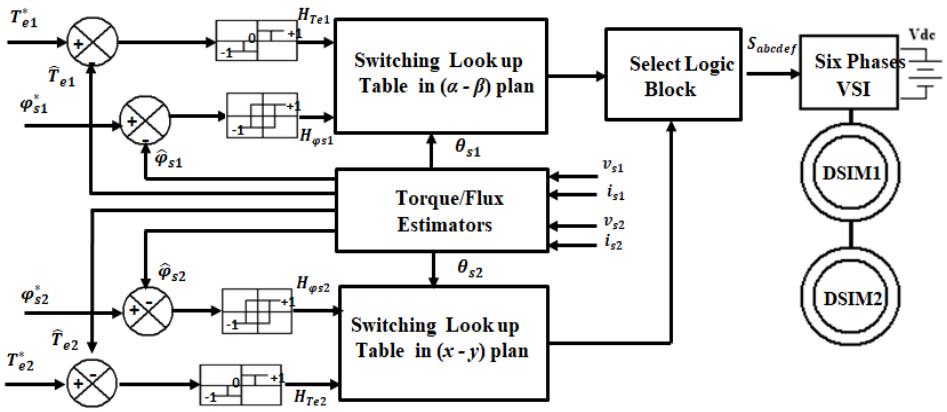

Figure 3: Conventional DTC block diagram.

To confirm our assumptions, a simulation was made first, aiming at the impact of the application of only the largest vectors on the shape of the currents feeding the two motors. An example of phase(a) current is shown in Figure 4, unsatisfactory results were obtained, that is, an amount of distortions can be observed which, consequently, will affects torque and flux variables, as a result, all the system drives efficiency. This is due mainly to the presence of non-producing torque/flux flowing in each machine simultaneously with the producing torque/flux components as explained in Section 1, therefore, to overcome this problem which degrades the performance controller, another strategy will be developed next.

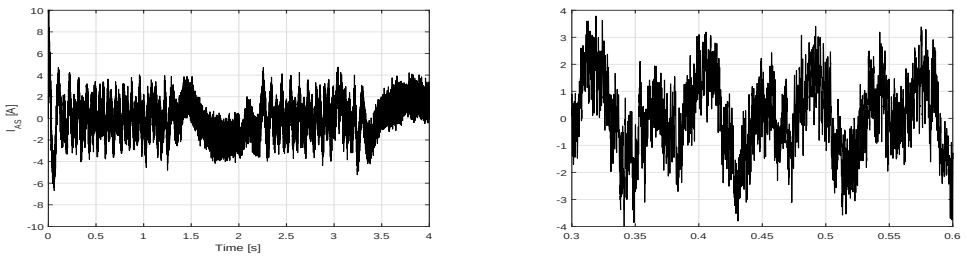

(a) (b)

Figure 4: Conventional DTC using only the largest vector : (a) inverter phase (a) current and (b) its zoomed snapshot.

3.2 Proposed DTC controller

The application of a large number of vectors of the subspace $(\alpha - \beta)$ and $(x - y)$ related to the current circulation, does not involve the production of couple / flux, but simply generate losses inside the system. To overcome these drawbacks, a DTC controller has been implemented to these components; benefiting from the possible advantages which ensue from it and which offer polyphase systems in terms of large number of space vectors. The diagram in Figure 5 illustrates the proposed controller.

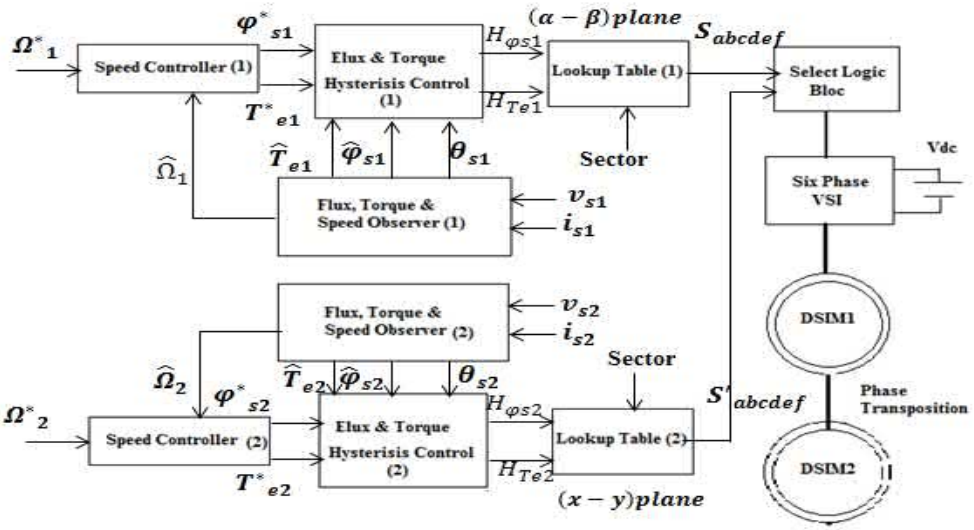

Figure 5: Proposed DTC block diagram.

The reason behind this technique is the vectors distribution, that is, by the help of Figure 2, one can observe the largest vectors in $(\alpha - \beta)$ plan appear as the smallest vectors in $(x - y)$ plan and vice versa, small and large vectors keep their magnitude but are shifted in each sub-space. Let us look, for example, at states 44, 64 and 66, the corresponding vectors v_{44}, v_{64} and v_{66} appear as the largest vectors in $(\alpha - \beta)$ plan while

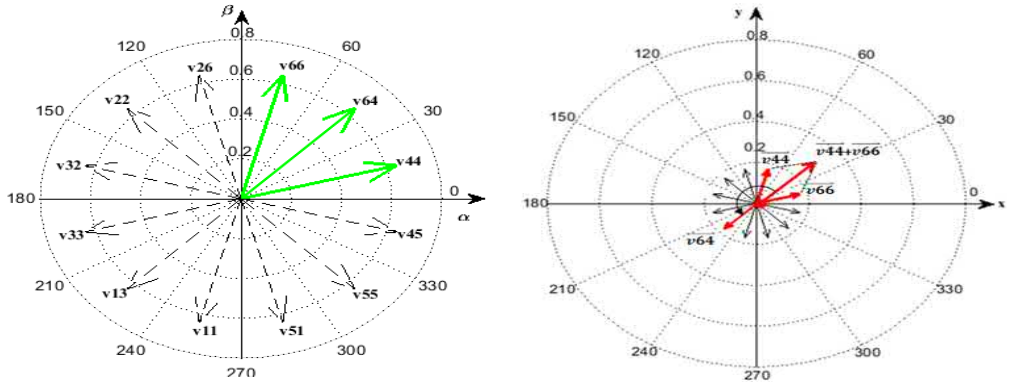

(a) (b)

Figure 6: Three largest vectors : (a) in $(\alpha - \beta)$ plan and (b) their projection in $(x - y)$ plan.

they appear as the smallest ones in $(x - y)$ plan where v_{64} is in opposite direction versus the vector sum of v_{44} and v_{66} as shown in Figure 6(b), therefore, to enforce the resultant of these vectors equal to zero mean volt- second product, the switching times should satisfy the following conditions:

$$|v_{44}|.\frac{t_1}{2} + |v_{64}|.\frac{t_1}{2} + |v_{66}|.t_2 = 0, \tag{10}$$

$$\frac{t_1}{2} + \frac{t_1}{2} + t_2 = T_s. \tag{11}$$

From (10) and (11), and taking into account the magnitude of vectors v_{44}, v_{64} and v_{66}, solving for t_1, t_2 (switching time of the applied vectors) gives

$$\frac{t_1}{2} \approx 0.25.T_s, \tag{12}$$

$$t_2 \approx 0.5.T_s. \tag{13}$$

The proposed technique will be extended to all vectors in each sub-space resulting in twelve active virtual vectors, i.e., $V_1 - V_{12}$, in $(\alpha - \beta)$ plan and twelve active virtual vectors from $(x - y)$ plan, i.e., $V_1^{'} - V_{12}^{'}$ as shown, respectively, in Figure 7 to synthesize two lookup tables identified with index '1' for the first motor and index '2' for the second motor in Figure 5. This selection of inverter states and dwell times should cancel current circulation which flows simultaneously with the energy producing components in each motor, as a result, less distortions in wave current forms and high performances of controller could be achieved within the drive system. If we consider the sector (1) indexed S1 in Figure 7(a), for example, to control the torque and flux of the first motor DSIM1, the voltage vector criterion is stated as follows. If the torque and flux have to be increased, i.e., $HT_{e1} = +1$ and $H\varphi_{s1} = +1$, the active virtual voltage V_2 or V_3 is selected; if the torque is to be increased and the flux is to be decreased, i.e., $H_{T_{e1}} = +1$ and $H\varphi_{s1} = -1$, then V_4 or V_5 is selected; if the torque is to be decreased and the flux is to be increased, i.e., $H_{T_{e1}} = -1$ and $H\varphi_{s1} = +1$, then V_{11} or V_{10} is selected; if the torque and flux have to be decreased, i.e., $H_{T_{e1}} = -1$ and $H\varphi_{s1} = -1$, then V_8 or V_9 is

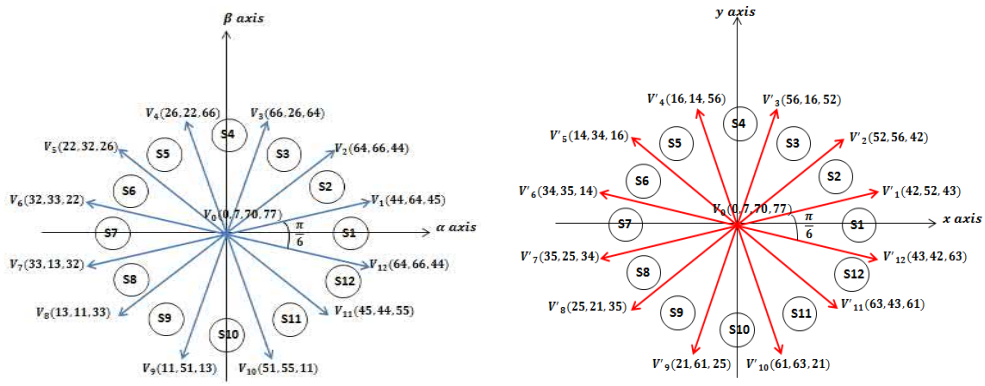

(a) (b)

Figure 7: Twelve active virtual voltage vectors and twelve sectors in (a) $(\alpha - \beta)$ plan and (b) $(x - y)$ plan.

selected; if the torque error is within the error band, i.e., $H_{T_{e1}} = 0$, the null voltage V_0 or V_{77} is selected regardless of the flux control loop. All cases are summarized in Table 1. The second voltage lookup table (not shown in this paper) will use $V_1^{'} - V_{12}^{'}$ from $(x-y)$ plan shown in Figure 7(b) to control the second motor DSIM2

$H_{\varphi_{s1}}$	$H_{T_{e1}}$	Sector number in $(\alpha - \beta)$ plan											
		I	*II*	*III*	*IV*	*V*	*VI*	*VII*	*VIII*	*IX*	*X*	*XI*	*XII*
+1	+1	V_2	V_3	V_4	V_5	V_6	V_7	V_8	V_9	V_{10}	V_{11}	V_{12}	V_1
		V_3	V_4	V_5	V_6	V_7	V_8	V_9	V_{10}	V_{11}	V_{12}	V_1	V_2
	-1	V_{11}	V_{12}	V_1	V_2	V_3	V_4	V_5	V_6	V_7	V_8	V_9	V_{10}
		V_{10}	V_{11}	V_{12}	V_1	V_2	V_3	V_4	V_5	V_6	V_7	V_8	V_9
-1	+1	V_5	V_6	V_7	V_8	V_9	V_{10}	V_{11}	V_{12}	V_1	V_2	V_3	V_4
		V_4	V_{16}	V_6	V_7	V_3	V_{43}	V_{41}	V_{61}	V_{60}	V_{70}	V_{30}	V_{34}
	-1	V_8	V_9	V_{10}	V_{11}	V_{12}	V_1	V_2	V_3	V_4	V_5	V_6	V_7
		V_9	V_{10}	V_{11}	V_{12}	V_1	V_2	V_3	V_4	V_5	V_6	V_7	V_8
+1	0	V_0	V_{77}	V_0	V_{77}	V_0	V_{77}	V_0	V_{77}	V_0	V_{77}	V_0	V_{77}
		V_0	V_{77}	V_0	V_{77}	V_0	V_{77}	V_0	V_{77}	V_0	V_{77}	V_0	V_{77}
-1	0	V_{77}	V_0	V_{77}	V_0	V_{77}	V_0	V_{77}	V_0	V_{77}	V_0	V_{77}	V_0
		V_{77}	V_0	V_{77}	V_0	V_{77}	V_0	V_{77}	V_0	V_{77}	V_0	V_{77}	V_0

Table 1: Voltage lookup table for DTC controller: shadowed part for low speed and unshaded part for high speed.

3.2.1 Derivation of flux and speed adaptive variable structure observer.

To provide motor's information for such control purposes, a derivative speed and flux observer is developed for DSIM1 based on the state-space model of the first motor DSIM1 given in (A.1), where

$\sigma_1 = 1 - \frac{L_{m1}^2}{L_{s1}L_{r1}}$, $T_{s1} = \frac{\sigma_1 L_{s1}+L_{ls2}}{(R_{s1}+R_{s2})}$ and $T_{r1} = \frac{L_{r1}}{R_{r1}}$,

$$p\underline{i}_{\alpha\beta s1} = \left(-\frac{1}{T_{s1}} - \frac{(1-\sigma_1)L_{s1}}{(\sigma_1 L_{s1}+L_{ls2})T_{r1}}\right)\underline{i}_{\alpha\beta s1} + \left(\frac{L_{m1}}{(\sigma_1 L_{s1}+L_{ls2})L_{r1}}\right)\left(\frac{1}{T_{r1}} - j\omega_{r1}\right)\underline{\phi}_{\alpha\beta r1} + \frac{1}{(\sigma_1 L_{s1}+L_{ls2})}\,\underline{v}_{\alpha\beta s1},$$

$$p\hat{\underline{i}}_{\alpha\beta s1} = \left(-\frac{1}{T_{s1}} - \frac{(1-\sigma_1)L_{s1}}{(\sigma_1 L_{s1}+L_{ls2})T_{r1}}\right)\hat{\underline{i}}_{\alpha\beta s1} + \left(\frac{L_{m1}}{(\sigma_1 L_{s1}+L_{ls2})L_{r1}}\right)\left(\frac{1}{T_{r1}} - j\hat{\omega}_{r1}\right)\hat{\underline{\phi}}_{\alpha\beta r1}, + \frac{1}{(\sigma_1 L_{s1}+L_{ls2})}\,\underline{v}_{\alpha\beta s1} + G_1 sign(\underline{i}_{\alpha\beta s1} - \hat{\underline{i}}_{\alpha\beta s1}) \tag{A-1}$$

$$\begin{aligned} p\underline{\phi}_{\alpha\beta r1} &= \frac{L_{m1}}{T_{r1}}\,\underline{i}_{\alpha\beta s1} + \left(\frac{1}{T_{r1}} - j\omega_{r1}\right)\underline{\phi}_{\alpha\beta r1}, \\ p\hat{\underline{\phi}}_{\alpha\beta r1} &= \frac{L_{m1}}{T_{r1}}\,\hat{\underline{i}}_{\alpha\beta s1} + \left(\frac{1}{T_{r1}} - j\hat{\omega}_{r1}\right)\hat{\underline{\phi}}_{\alpha\beta r1} + ... + \underline{G}_2 G_1 sign(\underline{i}_{\alpha\beta s1} - \hat{\underline{i}}_{\alpha\beta s1}). \end{aligned} \tag{A-2}$$

Subtracting (A.2) from (A.1) gives the error dynamics

$$p\Delta\underline{i}_{\alpha\beta s1} = \left(-\frac{1}{T_{s1}} - \frac{(1-\sigma_1)L_{s1}}{(\sigma_1 L_{s1}+L_{ls2})T_{r1}}\right)\underline{i}_{\alpha\beta s1} + \left(\frac{L_{m1}}{(\sigma_1 L_{s1}+L_{ls2})L_{r1}}\right)\left(\frac{1}{T_{r1}} - j\omega_{r1}\right)\underline{\phi}_{\alpha\beta r1} - \left(\frac{L_{m1}}{(\sigma_1 L_{s1}+L_{ls2})L_{r1}}\right) j\Delta\omega_{r1}\hat{\underline{\phi}}_{\alpha\beta r1} - G_1 sign(\Delta\underline{i}_{\alpha\beta s1}),$$

$$p\Delta\underline{\phi}_{\alpha\beta r1} = \frac{L_{m1}}{T_{r1}}\,\Delta\underline{i}_{\alpha\beta s1} - \left(\frac{1}{T_{r1}} - j\omega_{r1}\right)\Delta\underline{\phi}_{\alpha\beta r1} + j\Delta\omega_{r1}\hat{\underline{\phi}}_{\alpha\beta r1} - \underline{G}_2 G_1 sign(\Delta\underline{i}_{\alpha\beta s1}). \tag{A-3}$$

Provided that the scalar gain G1 is large enough, the equivalent component of the current error will converge to zero, such that $p\Delta\underline{i}_{\alpha\beta s1} = \Delta\underline{i}_{\alpha\beta s1} = 0$. Under this condition, the low frequency flux error dynamics is described by

$$\Delta\underline{\phi}_{\alpha\beta r1} = \left(j\Delta\omega_{r1}\hat{\underline{\phi}}_{\alpha\beta r1} + B\; G_1 sign(\Delta\underline{i}_{\alpha\beta s1})|_{eq}\right) \times \left(\frac{1}{T_{r1}} - j\omega_{r1}\right)^{-1}, \tag{A-4}$$

$$p\;\Delta\underline{\phi}_{\alpha\beta r1} = (B - \underline{G}_2)\, G_1 sign(\Delta\underline{i}_{\alpha\beta s1})|_{eq}, \tag{A-5}$$

where $B = \frac{L_{m1}\sigma_1}{1-\sigma_1}$. The positive definite Lyapunov candidate function V is chosen as in (A.6), with its time derivative $\dot{V}$ shown in (A.7).

$$V = \frac{1}{2}\left(\Delta\phi_{\alpha r1}^2 + \Delta\phi_{\beta r1}^2\right) + \frac{\Delta\omega_{r1}^2}{2\rho}, \quad \rho > 0, \tag{A-6}$$

$$\dot{V} = \Delta\underline{\phi}_{\alpha\beta r1}.\frac{d}{dt}\Delta\underline{\phi}_{\alpha\beta r1} + \frac{\Delta\omega_{r1}\frac{d}{dt}\Delta\omega_{r1}}{\rho} < 0. \tag{A-7}$$

Substituting (A.4) and (A.5) into (A.7) leads to (A.8). Negative definite $\dot{V} < 0$ is guaranteed if (A.9) is satisfied. The imaginary part in (A.9) is configured as zero to

avoid oscillation during error convergence. By solving (A.9) and replacing real speed with its estimated, the speed-dependent complex gain G2 can be determined as

$$\dot{V} = \underbrace{\left(B\ G_1 sign(\Delta \underline{i}_{\alpha\beta s1})|_{eq} \left(\frac{1}{T_{r1}} - j\omega_{r1}\right)^{-1}\right).\left((-B - G2)\ G_1 sign(\Delta \underline{i}_{\alpha\beta s1})|_{eq}\right)}_{\dot{V}<0}$$
$$+ \underbrace{\left(\Delta\omega_{r1} j\hat{\underline{\phi}}_{\alpha\beta r1} \left(\frac{1}{T_{r1}} - j\omega_{r1}\right)^{-1}\right)\left((-B - G2)\ G_1 sign(\Delta \underline{i}_{\alpha\beta s1})|_{eq}\right) + \frac{1}{\rho}\Delta\omega_{r1}\frac{d}{dt}\Delta\omega_{r1}}_{\dot{V}=0} \tag{A-8}$$

$$\frac{1}{B}(-B - \underline{G_2})\left(\frac{1}{T_{r1}} - j\omega_{r1}\right) = \mu, \quad \mu < 0. \tag{A-9}$$

By using (A.9) and considering $p\omega_{r1} = \frac{1}{J_1}\left(\hat{T}_{e1} - \hat{T}_{l1}\right)$, the speed adaptation law (A.10) can be determined from $\dot{V} = 0$ in (A.8)

$$\frac{d}{dt}\ \hat{\omega}_{r1} = K_\omega \left(sign(i_{\alpha s1} - \hat{i}_{\alpha s1})\hat{\phi}_{\beta r1} - sign(i_{\beta s1} - \hat{i}_{\beta s1})\right)\hat{\phi}_{\alpha r1} + \frac{\hat{T}_{e1} - \hat{T}_l}{J_1}, \qquad K_\omega > 0. \tag{A-10}$$

The electromagnetic torque is estimated by the deterministic model (A.8), and the load torque is estimated by an adaptation mechanism [13], as shown in (A.9):

$$\hat{T}_{e1} = 3\frac{P_1}{2}\frac{L_{m1}}{L_{r1}}\left(\hat{\phi}_{\alpha r1}\hat{i}_{\beta s1} - \hat{\phi}_{\beta r1}\hat{i}_{\alpha s1}\right), \tag{A-11}$$

$$\frac{d}{dt}\ \hat{T}_{l1} = -K_t\left(sign(i_{\alpha s1} - \hat{i}_{\alpha s1})\hat{\phi}_{\beta r1} - sign(i_{\beta s1} - \hat{i}_{\beta s1})\hat{\phi}_{\alpha r1}\right), \qquad K_t > 0. \tag{A-12}$$

Same procedure will be applied for DSIM2 to derive the flux and speed observer. The observer and controller parameters for each motor are: $G_1 = G_2 = 2000$, $\mu_1 = \mu_2 = -15$, $k_{w1} = 500$, $k_{w2} = 300$, $k_t = 50$, $F_{bw} = 0.02$, $T_{bw} = 2$.

4 System Synthesis and Simulation Results

In order to demonstrate the proposed DTC controller's performances adopted here in combination with the derived speed and flux observer, various simulations have been implemented as a comparative study to the conventional DTC controller, keeping the same motor and simulation parameters. For the conventional controller, only the largest virtual vectors have been used, while for the proposed one, the synthesized vectors shown in Table 1 are used, enabling the control of the drive system even at a low speed (shadowed part) or at a high speed (unshaded part), therefore, some figures are established, and then being compared to each other to reassert the performance of the proposed controller. In the appendix we show motor's parameters identified by index 1 and index 2 for DSIM1 and DSIM2, respectively. Additional bloc as shown in Figure 5 has been used to synthesize vector application of the proposed method and aims to alternatively keep flowing state signals generated from the lookup tables to inverter switches in each

half switching period. The model is discrete, good simulation results have been obtained with a 5 μs time step. The control system has two different sampling times : the speed controller sampling time has to be a multiple of the DTC sampling time, i.e., 50μs. The latter has to be a multiple of the simulation time step, i.e., 10μs. The following results are obtained for an exponential reference rotor speed from zero to 700 rpm for DSIM1 and from zero to 1400 rpm for DSIM2. Stator flux references for DSIM1 and DSIM2 are set, respectively, to 1Wb and 1.5 Wb and the dc-link voltage Vdc is set to 1000 Volt (2 Pu).

Figures 8 and 9 summarize the results of simulations for the system drive. Figure 8(a)

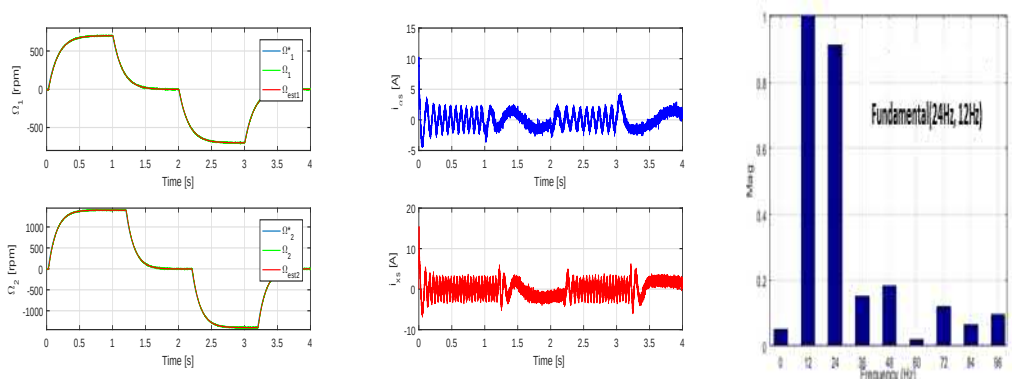

(a) (b) (c)

Figure 8: Proposed controller: (a) motor's speed, (b) $i_{\alpha s}$, i_{xs} inverter currents, (c) inverter currents spectrum.

shows both actual, estimated and reference speed under reversal speed transient with mechanical load (4 N.m) applied to DSIM1 and DSIM2 at 0.02s. Actual speeds follow precisely their references, as expected. Figure 8(b) and Figure 8(c) illustrate (α, β), (x, y) inverter currents and their harmonic spectrum, where we observe two different frequencies approximatively (24Hz and 12Hz). In Figure 9 and Figure 10, motor's torque and stator flux are shown, decoupled flux/torque for each machine within the whole system drive can be observed , in addition, less distortions can be seen in motor's torque with the proposed controller in Figure 9(a) if compared with Figure 9(b). Current waveforms of inverter phase (a) and their zoomed responses are shown in Figure 12 and Figure 13, respectively. One can observe a non sinusoidal waveform for both current responses, that is due to two different frequencies which provide the inverter to fed the system drive simultaneously running under different speed (700 and 1400 rpm). In Figure 12(b) an amount of distortions can be observed in the current waveform (without compensation of (x, y) components) if compared with the one obtained with the proposed DTC shown in Figure 12(a).

5 Conclusion

In this paper, the effectiveness and ability of controlling separately a two series connected quasi six-phase induction motor's drive fed by a single six-phase voltage source inverter (VSI), with an appropriate phase transposition based direct torque control (DTC), running under different working modes regardless of the torque and speed references, is

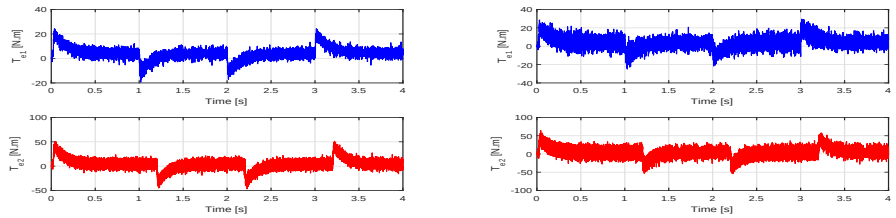

(a) (b)

Figure 9: Motor's torque: (a) proposed controller, (b) conventional controller.

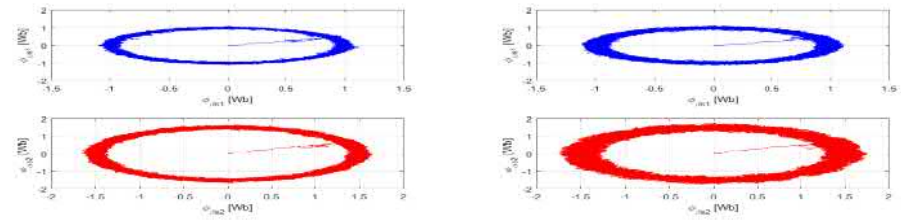

(a) (b)

Figure 10: Flux locus versus each other: (a) proposed controller, (b) conventional controller.

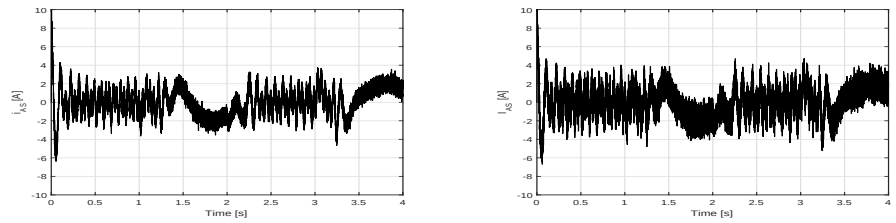

(a) (b)

Figure 11: Zoomed phase (a) current: (a) proposed controller, (b) conventional controller.

developed and verified by computer simulation. The technique is adopted under comparative analysis through the conventional controller and is possible via the usage of a large number of vectors that offers a multiphase system, in the minimization of machine's torque ripples and the controller's performance improvement by judicious voltage vectors selection. The cornerstone advantage of the proposed controller is the elimination of the harmonic current's low frequencies that make no contribution in producing of energy, but only generate extra losses within stator windings of the drive system, consequently, its efficiency is being degraded.

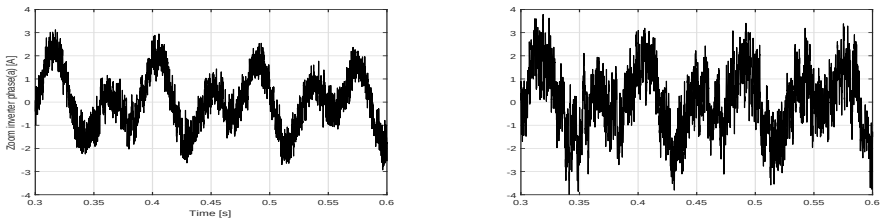

(a) (b)

Figure 12: Zoomed phase (a) current: (a) proposed controller, (b) conventional controller.

Acknowledgment

The research is part of a project PRFU'2020, realized respectively in the laboratory of electrical engineering and automatic LREA research, University of Medea, and Laboratory of Process Control (LCP), National Polytechnic School, Algiers, Algeria.

References

[1] E. Levi, M. Jones, S. N. Vukosavic and H. A. Toliyat. *A* novel concept of a multiphase, multi-motor vector controlled drive system supplied from a single voltage source inverter. *IEEE Trans. Power Electron.* **19**(2) (2004) 320–335.

[2] I. Zoric, M. Jones and E. Levi. *A*rbitrary Power Sharing Among Three-Phase Winding Sets of Multiphase Machines. *IEEE Trans. Ind. Electron.* **65**(2) (2018) 1128–1139.

[3] E. Levi. *A*dvances in Converter Control and Innovative Exploitation of Additional Degrees of Freedom for Multiphase Machines. *IEEE Trans. Ind. Electron.* **63**(5) (2016) 433–448.

[4] M.J. Duran and F. Barrero. *R*ecent Advances in the Design, Modeling, and Control of Multiphase Machines: Part II. *IEEE Trans. Ind. Electron.* **63**(3) (2016) 459–468.

[5] E. Levi, A. Iqbal, S. N. Vukosavic and H. A. Toliyat. Modeling and Control of a Five-Phase Series-Connected Two-Motor Drive. In: *The 29th Annual Conference of the IEEE Industrial Electronics Society (IECON)* **1**(1) (2003) 208–213.

[6] N.R. Abadji and D. Ghanbari. Direct torque and flux control of asymmetrical six-phase induction motor with zero sequence components elimination. *Rev. Roum. Sci. Techn. ectrotechn. et nerg.* **62**(1) (2017) 63–41.

[7] E. Daryabeigi, N.R. Abjadi and G.R. Arab Markadeh. Automatic speed control of an asymmetrical six-phase induction motor using emotional controller *Journal of Intelligent Fuzzy Systems* BELBIC **26**(4) (2013) 1879–1892.

[8] A. Azib, D. Ziane, T. Rekioua and A. Tounzi. Robustness of the direct torque control of double star induction motor in falut condition. *Rev. Roum. Sci. Techn. ectrotechn. et nerg.* **61**(2) (2016) 147–152.

[9] E. Benyoussef, A. Meroufel and S. Barkat. Neural network and fuzzy logic direct torque control of sensorless double star synchronous machine. *Rev. Roum. Sci. Techn. ectrotechn. et nerg.* **61**(3) (2016) 239–243.

[10] G. Sheng-wei and C. Yan. *R*esearch on torque ripple minimization strategy for direct control of induction motors. In: *Proc. ICCASM* (2010) 278–281.

[11] Libo Zheng, John E. Fletcher, Barry W. Williams and Xiangning He. A novel direct torque control scheme for a sensorless five-phase induction motor drive. *IEEE Transactions on industrial electronics.* **58**(2) (2011) 503–513.

[12] J. Soltani, N. R. Abjadi, Gh. R. Arab Markadeh and H. W. Ping. Adaptive sliding-mode control of a two five-phase series-connected induction motors drive. *Proceeding of International Conference on Electrical Machines and Systems.* (2007), Oct. 8-11, Seoul, Korea.

[13] Masood Hajian, Jafar Soltani, Gholamreza Arab Markadeh and Saeed Hosseinnia. Adaptive Nonlinear Direct Torque Control of Sensorless IM Drives With Efficiency Optimization. *IEEE Trans. Ind. Electron.* **57**(3) (2010) 975–985.

[14] F. Hamidia, A. Abadi, A. Tlemcani and M. S. Boucherit. Dual star induction motor supplied with double photovoltaic panels based on fuzzy logic type–2.*Nonlinear Dynamics and Systems Theory* **18**(4) (2018) 359–371.

[15] S. Boulkhrachef, A. Moualdia, Dj. Boudana and P. Wira. Higher-order sliding mode control of a wind energy conversion system. *Nonlinear Dynamics and Systems Theory* **19**(4) (2019) 486–496.

[16] A.G. Mazko. Robust output feedback stabilization and optimization of discrete-time control systems.*Nonlinear Dynamics and Systems Theory* **18**(1) (2018) 92–106.

[17] Djamel Boudana, Lazhari Nezli, Mohand Oulhadj Mahmoudi and Mohame Tadjne. Robust dtc based on adaptive fuzzy control of double star synchronous machine drive with fixed switching frequency. *Journal of Electrical Engineering* **63**(3) (2012) 133–143.

[18] A. Moualdia, M. O. Mahmoudi and L. Nezli.*D*irect Torque Control of the DFIG and Direct Power Control for Grid Side Converter in wind power generation system. *The Mediterranean Journal of Measurement and Control, MEDJMC* **9**(3) (2013) 101–108.

[19] A. Chalanga, S. Kamal and B. Moreno. *I*mplementation of super-twisting control: super-twisting and higher Order sliding-mode observer-based approaches. *IEEE Trans. on Industrial Electronics* **63** (6) (2016) 3677–3685.

Appendix

DSIM1 and DSIM2 Parameters

Parameters	DSIM1	DSIM2
Stator resistance	$R_{s1} = 9\Omega$	$R_{s2} = 9\Omega$
Rotor resistance	$R_{r1} = 8.37\Omega$	$R_{r2} = 8.37\Omega$
Stator inductance	$L_{s1} = 740mH$	$L_{s2} = 740mH$
Rotor inductance	$L_{r1} = 740mH$	$L_{r2} = 740mH$
Mutual inductance	$L_{m1} = 712mH$	$L_{m2} = 712mH$
Number of pole	$P_1 = 4$	$P_2 = 4$
Moment of inertia	$J_1 = 0.066Kg.m^2$	$J_2 = 0.066Kg.m^2$
Friction coefficient	$B_1 = 0.001N.m.s/rd$	$B_2 = 0.001N.m.s/rd$